International Journal of Solids and Structures 45 (2008) 5814–5830

Contents lists available at ScienceDirect

International Journal of Solids and Structures

journal homepage: www.elsevier.com/locate/ijsolstr

Analytical solution of the contact problem of a rigid indenter and an anisotropic linear elastic layer

R.C. Batra *, W. Jiang

Department of Engineering Science and Mechanics, M/C 0219, Virginia Polytechnic Institute & State University, Blacksburg, VA 24061, USA

ARTICLE INFO

Article history:
Received 7 March 2008
Received in revised form 12 June 2008
Available online 28 June 2008

Keywords:
Analytical solution
Cylindrical indenter
Orthotropic layer
General anisotropic layer
Flat punch

ABSTRACT

We use the Stroh formalism to study analytically generalized plane strain deformations of a linear elastic anisotropic layer bonded to a rigid substrate, and indented by a rigid cylindrical indenter. The mixed boundary-value problem is challenging since the a priori unknown deformed indented surface of the layer contacting the rigid cylinder is to be determined as a part of the solution of the problem. For a rigid parabolic prismatic indenter contacting either an isotropic layer or an orthotropic layer and a flat rigid punch indenting a half space, the computed solutions are found to agree well with those available in the literature. Parametric studies have been conducted to delimit the length and the thickness of the layer for which the derived relation between the axial load and the indentation depth caused by the rigid cylinder is valid. The indentation of a face centered cubic crystal with the plane of indentation oriented differently from the principal planes of symmetry has also been studied to illustrate the applicability of the technique to general layers made of anisotropic materials. Results presented herein can serve as benchmarks with which to compare solutions obtained by other methods.

© 2008 Elsevier Ltd. All rights reserved.

1. Introduction

Thin films are used in numerous applications such as protective surfaces in artificial joints, underfills in flip chip technology, and coatings on optical equipment and turbine blades. Mechanical properties of thin films and nanosize objects are usually measured with an indentation test, and the value of the elastic modulus in the indentation direction is extracted from the slope of the load versus indentation depth curve. These tests are also used to determine elastic moduli of articular cartilage (Töyräs et al., 2001) which can provide useful information about the health of the tissue especially when these tests are done in vivo. At the other extreme, similar mechanics issues arise in contact problems of bearings with rubber linings, photocopying machines, and in the textile and paper machinery where a cylinder coated with a layer of rubberlike material either contacts a steel cylinder or another steel cylinder coated with a rubberlike material. Depending upon dimensions of the indenter, the layer, and the contact zone, the problem may be analyzed as either plane stress, plane strain or as three-dimensional (3D). A 3D problem is usually studied numerically.

In many applications Young's modulus of the indenter material is significantly higher than that of the material of the elastic layer being indented, and the indenter can be regarded as rigid. This is certainly true for the indentation of a soft tissue, and for rollers used in the paper and the textile industries. Furthermore, the deformable layer is usually bonded to a material that may also be regarded as rigid. When indentation depth is small in comparison to the thickness of the deformable layer, the radius of the indenter, and the width of the layer, the response of the material of the layer may be regarded as linear

* Corresponding author. Tel.: +1 5402316051; fax: +1 5402314574.
E-mail addresses: rbatra@vt.edu (R.C. Batra), wjiang@vt.edu (W. Jiang).

0020-7683/$ - see front matter © 2008 Elsevier Ltd. All rights reserved.
doi:10.1016/j.ijsolstr.2008.06.016

elastic. Contact problems for even linear elastic materials are challenging because, in general, the shape of the contact area and the pressure distribution on it are unknown a priori. The problem formulation usually involves mixed boundary conditions of normal displacements prescribed on the contact area and null surface tractions on the free boundary surface close to the indenter but not contacting it. The complexity of the problem increases with an increase in the degree of anisotropy of the material of the indented layer. Analytical solutions of linear problems for isotropic materials with different approximations have been summarized by Johnson (1985) and several references are cited therein. Whereas two elastic moduli characterize a linear elastic isotropic material, the number of elastic moduli for a face centered cubic, a transversely isotropic, and an orthotropic material equal 3, 5 and 9, respectively. Both the analysis of the contact problem and the identification of material moduli from test results become more challenging when the layer material is anisotropic.

Contact problems for transversely isotropic materials have been investigated by Green and Zerna (1954) and Turner (1966). Willis (1966) employed the double Fourier transform technique to analyze the Hertz contact problem for a transversely isotropic half space. Swanson (2004) used Willis's method of double Fourier transforms to reduce governing coupled partial differential equations for the three displacement components to ordinary differential equations which involve derivatives with respect to the coordinate in the indentation direction. Assuming that each displacement component has the same exponential variation in the indentation direction, the problem is reduced to solving a system of three simultaneous algebraic equations. By assuming that edges of the indented layer are simply supported, which is usually not the case for a layer bonded to a rigid substrate, Swanson (2004) found displacement and stress distributions within the layer by using an approach similar to that of Srinivas and Rao (1970). Swanson (2004) compared the computed solution with that of Turner (1966) for transversely isotropic materials, and also provided solutions for orthotropic materials. Swanson (2004) asserted that the solution technique can not be adopted for general anisotropic materials because Srinivas and Rao (1970) gave Green's function only for orthotropic materials.

Swadener and Pharr (2001) simplified Willis's (1966) method by using the surface Green function derived earlier by Barnett and Lothe (1975), and studied the indentation of an anisotropic half-space by rigid frictionless parabolic and conical indenters. Fan and Hwu (1996), Hwu and Fan (1998), Ning et al. (2003), and Lin and Ovaert (2004) have combined Stroh's formalism with the analytical continuation (Muskhelishvili, 1954) and the conjugate gradient methods to study indentation of an anisotropic half space by rough indenters of arbitrary profiles. Aboussaleh and Boukhili (1998) have analyzed the contact between a composite laminate and a rigid indenter by assuming that the laminate has a plane of elastic symmetry parallel to its mid-surface and the variation of stresses through the laminate thickness in known. Wu and Yen (1994) employed Green's function to investigate the contact between a simply supported orthotropic plate and a rigid sphere. Based on experimental results, Yang and Sun (1982) and Tan and Sun (1985) modified the Hertz contact law for an orthotropic layer by assuming that the pressure distribution on the contact surface and the width of the contact area for an anisotropic layer can be derived from those for an isotropic layer by replacing Young's modulus by the elastic modulus of the anisotropic layer in the indentation direction. It seems that the indentation of an anisotropic layer of finite width and thickness has not been studied analytically.

Kuo and Keer (1992) analyzed the contact of a rigid spherical indenter with a half space comprised of several perfectly bonded layers of transversely isotropic materials. By employing Hankel transforms, the mixed boundary-value problem was reduced to an integral equation that was solved numerically for tractions and displacements on the contact region. Lovell and Morrow (2006) have used the finite element method to analyze 3D deformations of a spherical indenter normally loaded between two flat layers made of transversely isotropic materials. They synthesized results for numerous case studies to provide empirical relations between the contact stress and the indentation depth.

Here, we adopt Stroh's formalism (1958, 1962) to study infinitesimal deformations of an anisotropic layer of finite width and thickness perfectly bonded to a rigid substrate and indented by an indenter of arbitrary profile with the goal of deriving a relation between the axial load and the indentation depth. The analytical function in Stroh's formalism is expressed as Fourier's sine and cosine series with their coefficients decaying exponentially in the thickness direction; e.g. see Vel and Batra (2000) who used this technique to analyze deformations of an anisotropic plate under different boundary conditions. The unknown constants in the Fourier series are determined by satisfying boundary conditions in an average sense. The convergence of the series solution is established by solving two contact problems; one for an isotropic and the other for an orthotropic layer and comparing their solutions with results available in the literature. Subsequently, parametric studies are performed to delineate the effect of various material and geometric parameters upon the load required to indent an orthotropic layer by a prescribed amount. Finally, the indentation of a linear elastic anisotropic layer by a flat indenter is studied.

2. Problem formulation

The problem studied, shown schematically in Fig. 1, involves a linear elastic, homogeneous and anisotropic layer bonded to a rigid substrate and indented by a rigid circular cylinder. It is assumed that the length of the cylinder and of the layer in the x_2-direction (perpendicular to the plane of the paper) is very large as compared to dimensions of the layer within the plane of the paper (i.e., the length L, and the thickness h of the layer). We assume that the indentation depth is such as to induce infinitesimal deformations of the layer. As the cylinder is pressed statically into the linear elastic layer, points of the layer underneath the cylinder move vertically down, those not on the axis of the cylinder also move axially outwards while those near the free surface of the layer and adjacent to the rigid cylinder move upwards. We denote indentation of the cylinder into the layer by u_0, and the semi-contact width by c; u_0 and c are depicted in Fig. 1.

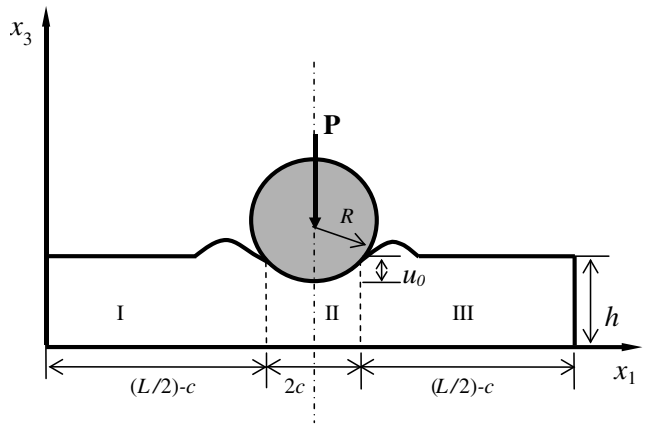

Fig. 1. Schematic sketch of the problem studied.

We use rectangular Cartesian coordinates to describe infinitesimal deformations of the layer, and assume that the displacement field **u** and hence stresses and strains induced in the layer are functions of x_1 and x_3 only. Thus the state of deformation of the layer corresponds to that of generalized plane strain. In the absence of body forces, equations governing deformations of the layer are

$$\sigma_{ij,j} = 0, \quad i = 1,2,3, \tag{1}$$

$$\sigma_{ij} = C_{ijkl} e_{kl}, \quad C_{ijkl} = C_{jikl} = C_{klij}, \tag{2}$$

$$e_{kl} = \frac{1}{2}(u_{k,l} + u_{l,k}), \tag{3}$$

where $\sigma_{ij} = \sigma_{ji}$ is the Cauchy stress tensor, $\sigma_{ij,j} = \partial\sigma_{ij}/\partial x_j$, a repeated index implies summation over the range of the index, e_{kl} is the infinitesimal strain tensor, u_i is the displacement of a point in the x_i-direction, and C_{ijkl} is an elastic constant of the material of the linear elastic layer. Symmetries indicated in Eq. (2) imply that, for a 3D problem, C_{ijkl} can be written as a symmetric 6×6 matrix, and σ_{ij} and e_{kl} as 6×1 matrices. Henceforth, we assume that C_{ijkl} is positive-definite which is equivalent to presuming that the strain energy density is positive for every non-rigid deformation of the body.

Substitution from Eq. (3) into Eq. (2), and the result into Eq. (1) yields the following second-order coupled partial differential equations for u_1, u_2 and u_3:

$$C_{ijkl} u_{l,kj} = 0, \quad i = 1,2,3. \tag{4}$$

Pertinent boundary conditions are:

$$\sigma_{11} = \sigma_{31} = 0 \quad \text{on } x_1 = 0, L, \tag{5a}$$

$$u_1 = u_3 = 0 \quad \text{on } x_3 = 0, \tag{5b}$$

$$\sigma_{13} = \sigma_{33} = 0 \quad \text{on } x_3 = h \quad \text{and} \quad |x_1 - L/2| > c, \tag{5c}$$

$$(\mu \sin^2\theta + \sin\theta\cos\theta)\sigma_{11} - (\mu \sin 2\theta + \cos 2\theta)\sigma_{31} + (\mu\cos^2\theta - \sin\theta\cos\theta)\sigma_{33} = 0,$$

$$u_3 = g(x_1) \quad \text{on } x_3 = h \quad \text{and} \quad |x_1 - L/2| \leqslant c. \tag{5d}$$

Here, $\theta = \arcsin((x_1 - L/2)/R)$, μ is the coefficient of friction between the rigid indenter and the deformable layer, and the function $g(x_1)$ depends upon the shape of the indenter. In cylindrical coordinates, the left-hand side of Eq. $(5d)_1$ equals $(\sigma_{r\theta} - \mu\sigma_{rr})$, where $\sigma_{r\theta}$ and σ_{rr} are, respectively, the tangential and the normal tractions at a point on the contact surface. When the contact surface between the indenter and the deformable layer can be regarded as smooth, $\mu = 0$. Points of the contact surface where $\sigma_{rr} \geqslant 0$ do not contact the indenter. We assume that there is no separation between the indenter and the deformable layer; thus the contact surface is contiguous. For a rigid circular cylinder of radius R,

$$g(x_1) = R - u_0 - \sqrt{R^2 - (x_1 - L/2)^2}, \tag{6}$$

where u_0 is the indentation (e.g. see Fig. 1). In a 3D problem, boundary conditions on end faces parallel to the x_1x_3-plane also need to be specified.

We study infinitesimal deformations of the layer, hence $c/R \ll 1$. Disregarding the curvature of the cylinder, we write the axial load P per unit length of the cylinder as

$$P = -\int_{L/2-c}^{L/2+c} \sigma_{33}\, \mathrm{d}x_3. \tag{7a}$$

If curvature of the cylinder is considered, then

$$P = -\int_{L/2-c}^{L/2+c} (\sigma_{33} - \sigma_{13}\tan\theta)\mathrm{d}x_3. \tag{7b}$$

Out of three variables P, c and u_0 characterizing the indentation of the cylinder into the layer, only one can be specified, and the other two are determined as a part of the solution of the problem. Here, we prescribe c and find corresponding values of P and u_0.

3. Analytical solution of the problem

Following Fan and Hwu (1996), Hwu and Fan (1998), and Vel and Batra (2000) we use the Stroh formalism to find a general solution of the above formulated mixed boundary-value problem. Accordingly, we divide the deformable layer into three regions I, II and III as exhibited in Fig. 1. The region I extends from the left edge $x_1 = 0$ of the layer to the vertical surface $x_1 = (L/2) - c$ that passes through the left-most contact point, the region II of width $2c$ is directly under the contact surface, and region III extends from $x_1 = (L/2) + c$ to the right edge $x_1 = L$ of the layer. We require that displacements and surface tractions be continuous across the interface between regions I and II, and the interface between regions II and III. That is, $i = 1,2,3$,

$$u_i((L/2-c)^-, x_3) - u_i((L/2-c)^+, x_3) = 0, \tag{8a}$$
$$u_i((L/2+c)^-, x_3) - u_i((L/2+c)^+, x_3) = 0, \tag{8b}$$
$$\sigma_{i1}((L/2-c)^-, x_3) - \sigma_{i1}((L/2-c)^+, x_3) = 0, \tag{8c}$$
$$\sigma_{i1}((L/2+c)^-, x_3) - \sigma_{i1}((L/2+c)^+, x_3) = 0. \tag{8d}$$

While finding a general solution of the governing equations, we assume that

$$u_i = a_i f(z), \quad z = x_1 + p x_3, \quad i = 1,2,3, \tag{9}$$

where f is an arbitrary analytic function of z, and a_1, a_2, a_3 and p are complex numbers to be determined. Substitution for u_i from Eq. (9) into Eq. (4) yields

$$[C_{i11l} + p(C_{i13l} + C_{i31l}) + p^2 C_{i33l}]a_l = 0, \tag{10}$$

where we have assumed that $f'(z) = \mathrm{d}^2 f/\mathrm{d}z^2 \neq 0$. We define 3×3 matrices $\mathbf{Q}$, $\mathbf{R}$ and $\mathbf{T}$ as follows:

$$Q_{il} = C_{i11l}, \quad R_{il} = C_{i13l}, \quad T_{il} = C_{i33l}. \tag{11}$$

Using symmetries of the elasticity matrix C_{ijkl} indicated in Eq. (2), we write the eigenvalue problem defined by Eq. (10) in direct notation as

$$[\mathbf{Q} + p(\mathbf{R} + \mathbf{R}^{\mathrm{T}}) + p^2\mathbf{T}]\mathbf{a} = \mathbf{0}. \tag{12}$$

The positive-definiteness of $\mathbf{C}$ implies that $\mathbf{Q}$ and $\mathbf{T}$ are positive-definite matrices. With the definition

$$\mathbf{b} = -\frac{1}{p}(\mathbf{Q} + p\mathbf{R})\mathbf{a} = (\mathbf{R}^{\mathrm{T}} + p\mathbf{T})\mathbf{a}, \tag{13}$$

the eigenvalue problem defined by Eq. (12) can be written as

$$\mathbf{N}\boldsymbol{\zeta} = p\boldsymbol{\zeta}, \tag{14}$$

where

$$\mathbf{N} = \begin{bmatrix} -\mathbf{T}^{-1}\mathbf{R}^{\mathrm{T}} & \mathbf{T}^{-1} \\ \mathbf{R}\mathbf{T}^{-1}\mathbf{R}^{\mathrm{T}} - \mathbf{Q} & -\mathbf{R}\mathbf{T}^{-1} \end{bmatrix}, \quad \boldsymbol{\zeta} = \begin{Bmatrix} \mathbf{a} \\ \mathbf{b} \end{Bmatrix}, \tag{15}$$

p is the eigen-value and $\boldsymbol{\zeta}$ the eigen-vector. For the strain energy density to be positive definite, p must be complex (Eshelby et al., 1953). Let (p_α, a_α), $\alpha = 1,2,\ldots,6$ be eigensolutions of Eq. (12) such that

$$\mathrm{Im}(p_\alpha) > 0, \quad p_{\alpha+3} = \bar{p}_\alpha, \quad a_{\alpha+3} = \bar{a}_\alpha, \quad \alpha = 1,2,3, \tag{16}$$

where $\bar{p}_\alpha$ is the complex conjugate of p_α. Assuming that all p's are distinct, a general solution of Eqs. (1)–(3) can be written as

$$\mathbf{u} = \sum_{\alpha=1}^{3} [\mathbf{a}_\alpha f_\alpha(z_\alpha) + \bar{\mathbf{a}}_\alpha f_{\alpha+3}(\bar{z}_\alpha)], \tag{17}$$

where f_α ($\alpha = 1,2,\ldots,6$) are arbitrary analytic functions of z_α. The general solution (17) holds even when the six eigenvalues are not distinct but there exist six linearly independent eigenvectors. Ting (1996) has discussed how to modify the general solution when the eigenvalue problem defined by Eq. (12) does not have six linearly independent eigenvectors.

Substitution for $\mathbf{u}$ from Eq. (17) into Eq. (3) and the result into Eq. (2) gives

$$\boldsymbol{\sigma}_1 = -\sum_{\alpha=1}^{3}[p_\alpha \mathbf{b}_\alpha f'_\alpha(z_\alpha) + \bar{p}_\alpha \bar{\mathbf{b}}_\alpha f'_{\alpha+3}(\bar{z}_\alpha)], \tag{18}$$

$$\boldsymbol{\sigma}_3 = -\sum_{\alpha=1}^{3}[\mathbf{b}_\alpha f'_\alpha(z_\alpha) + \bar{\mathbf{b}}_\alpha f'_{\alpha+3}(\bar{z}_\alpha)], \tag{19}$$

where

$$(\boldsymbol{\sigma}_1)_i = \sigma_{i1}, \quad (\boldsymbol{\sigma}_3)_i = \sigma_{i3}. \tag{20}$$

We note that $\boldsymbol{\sigma}$ given by Eq. (18) satisfies the equilibrium equation (1) for all choices of the analytic function $f_\alpha(z)$. In order to satisfy boundary conditions (5) and continuity conditions (8) we assume the following series solution for the nth ($n = 1,2,3$) region:

$$f_\alpha^{(n)}(z_\alpha^{(n)}) = d_\alpha^{(n)} + z_\alpha^{(n)} v_\alpha^{(n)} + (z_\alpha^{(n)})^2 w_\alpha^{(n)} + \sum_{k=1}^{\infty}\left\{q_{k\alpha}^{(n)} \exp(\lambda_{k\alpha}^{(n)} z_\alpha^{(n)}) + r_{k\alpha}^{(n)} \exp(\lambda_{k\alpha}^{(n)}(p_\alpha^{(n)} h - z_\alpha^{(n)}))\right\}$$
$$+ \sum_{m=1}^{\infty}\left\{s_{m\alpha}^{(n)} \exp(\eta_{m\alpha}^{(n)} z_\alpha^{(n)}) + t_{m\alpha}^{(n)} \exp(\eta_{m\alpha}^{(n)}(l^{(n)} - z_\alpha^{(n)}))\right\}, \quad 0 \leqslant x_1^{(n)} \leqslant l^{(n)}, \tag{21}$$

where

$$z_\alpha^{(n)} = x_1^{(n)} + p_\alpha^{(n)} x_3^{(n)}, \quad \lambda_{k\alpha}^{(n)} = \frac{k\pi i}{l^{(n)}}, \quad \eta_{m\alpha}^{(n)} = -\frac{m\pi i}{p_\alpha^{(n)} h}, \quad i = \sqrt{-1}. \tag{22}$$

The unknowns $d_\alpha^{(n)}$ and $w_\alpha^{(n)}$ are assumed to be real while $v_\alpha^{(n)}$, $q_{k\alpha}^{(n)}$, $r_{k\alpha}^{(n)}$, $s_{m\alpha}^{(n)}$ and $t_{m\alpha}^{(n)}$ are complex; these will be determined from boundary conditions, and continuity conditions at the interfaces. In Eqs. (21) and (22), $l^{(n)}$ ($n = 1,2,3$) is the width of the n^{th} segment, and $x_1^{(n)}$ is the x_1-coordinate of a point in the n^{th} segment measured from the left edge of the segment. Note that each term in series (21) is an analytical function of $z_\alpha^{(n)}$. The choice (21) for $f_\alpha(z)$ is dictated by shapes of segments.

Substituting for $f_\alpha(z_\alpha)$ from Eq. (21) into Eqs. (17)–(19), we get the following for the displacements $\mathbf{u}^{(n)}$ and stresses $\boldsymbol{\sigma}_1^{(n)}$ and $\boldsymbol{\sigma}_3^{(n)}$ in the n^{th} segment:

$$\mathbf{u}^{(n)} = \mathbf{A}\Bigg\{\mathbf{d}^{(n)} + \langle z_*^{(n)}\rangle \mathbf{v}^{(n)} + \left\langle (z_*^{(n)})^2\right\rangle \mathbf{w}^{(n)} + \sum_{k=1}^{\infty}\left[\left\langle \exp(\beta_{k*}^{(n)})\right\rangle \mathbf{q}_k^{(n)} + \left\langle \exp(\gamma_{k*}^{(n)})\right\rangle \mathbf{r}_k^{(n)}\right]$$
$$+ \sum_{m=1}^{\infty}\left[\left\langle \exp(\delta_{m*}^{(n)})\right\rangle \mathbf{s}_m^{(n)} + \left\langle \exp(\xi_{m*}^{(n)})\right\rangle \mathbf{t}_k^{(n)}\right]\Bigg\} + \text{conjugate}, \tag{23}$$

$$\boldsymbol{\sigma}_1^{(n)} = \mathbf{B}\Bigg\{-\langle p_*^{(n)}\rangle \mathbf{v}^{(n)} - \langle 2p_*^{(n)} z_*^{(n)}\rangle \mathbf{w}^{(n)} + \sum_{k=1}^{\infty}\left[-\left\langle \lambda_{k*}^{(n)} p_*^{(n)} \exp(\beta_{k*}^{(n)})\right\rangle \mathbf{q}_k^{(n)} + \left\langle \lambda_{k*}^{(n)} p_*^{(n)} \exp(\gamma_{k*}^{(n)})\right\rangle \mathbf{r}_k^{(n)}\right]$$
$$+ \sum_{m=1}^{\infty}\left[-\left\langle \eta_{m*}^{(n)} p_*^{(n)} \exp(\delta_{m*}^{(n)})\right\rangle \mathbf{s}_m^{(n)} + \left\langle \eta_{m*}^{(n)} p_*^{(n)} \exp(\xi_{m*}^{(n)})\right\rangle \mathbf{t}_k^{(n)}\right]\Bigg\} + \text{conjugate}, \tag{24}$$

$$\boldsymbol{\sigma}_3^{(n)} = \mathbf{B}\Bigg\{\mathbf{v}^{(n)} + \langle 2z_*^{(n)}\rangle \mathbf{w}^{(n)} + \sum_{k=1}^{\infty}\left[\left\langle \lambda_{k*}^{(n)} \exp(\beta_{k*}^{(n)})\right\rangle \mathbf{q}_k^{(n)} - \left\langle \lambda_{k*}^{(n)} \exp(\gamma_{k*}^{(n)})\right\rangle \mathbf{r}_k^{(n)}\right]$$
$$+ \sum_{m=1}^{\infty}\left[\left\langle \eta_{m*}^{(n)} \exp(\delta_{m*}^{(n)})\right\rangle \mathbf{s}_m^{(n)} - \left\langle \eta_{m*}^{(n)} \exp(\xi_{m*}^{(n)})\right\rangle \mathbf{t}_k^{(n)}\right]\Bigg\} + \text{conjugate}, \tag{25}$$

where

$$\mathbf{A} = [\mathbf{a}_1\ \mathbf{a}_2\ \mathbf{a}_3], \quad \mathbf{B} = [\mathbf{b}_1\ \mathbf{b}_2\ \mathbf{b}_3],$$
$$\beta_{k\alpha}^{(n)} = \lambda_{k\alpha}^{(n)} z_\alpha^{(n)}, \quad \gamma_{k\alpha}^{(n)} = \lambda_{k\alpha}^{(n)}(p_\alpha^{(n)} h - z_\alpha^{(n)}),$$
$$\delta_{m\alpha}^{(n)} = \eta_{m\alpha}^{(n)} z_\alpha^{(n)}, \quad \xi_{m\alpha}^{(n)} = \eta_{m\alpha}^{(n)}\left(l^{(n)} - z_\alpha^{(n)}\right),$$
$$\langle \phi_*\psi_*\chi_*\rangle = \text{diag}[\phi_1\psi_1\chi_1, \phi_2\psi_2\chi_2, \phi_3\psi_3\chi_3],$$
$$(\mathbf{d}^{(n)})_\alpha = d_\alpha^{(n)}, \quad \alpha = 1,2,3. \tag{26}$$

The unknowns $\mathbf{d}^{(n)}$ and $\mathbf{w}^{(n)}$ are assumed to be real while $\mathbf{v}^{(n)}$, $\mathbf{q}_k^{(n)}$, $\mathbf{r}_k^{(n)}$, $\mathbf{s}_m^{(n)}$, $\mathbf{t}_m^{(n)}$ are complex and defined in a way similar to $\mathbf{d}^{(n)}$, and conjugate stands for the complex conjugate of the explicitly stated terms.

In terms of the 3×3 diagonal matrices $\mathbf{I}_u^l$, $\mathbf{I}_\sigma^l$, $\mathbf{I}_u^r$, $\mathbf{I}_\sigma^r$, $\mathbf{I}_u^t$, $\mathbf{I}_\sigma^t$, $\mathbf{I}_u^b$, $\mathbf{I}_\sigma^b$ whose elements are constants, and

$$\mathbf{I}_u^l+\mathbf{I}_\sigma^l=\mathbf{I}_u^r+\mathbf{I}_\sigma^r=\mathbf{I}_u^t+\mathbf{I}_\sigma^t=\mathbf{I}_u^b+\mathbf{I}_\sigma^b=\mathbf{I}, \tag{27}$$

where $\mathbf{I}$ is the 3×3 identity matrix, boundary conditions (5) with $\mu=0$ can be written as

$$\mathbf{I}_u^l\mathbf{u}+\mathbf{I}_\sigma^l\boldsymbol{\sigma}_1=\mathbf{0} \quad \text{on } x_1=0, \tag{28a}$$
$$\mathbf{I}_u^r\mathbf{u}+\mathbf{I}_\sigma^r\boldsymbol{\sigma}_1=\mathbf{0} \quad \text{on } x_1=L, \tag{28b}$$
$$\mathbf{I}_u^b\mathbf{u}+\mathbf{I}_\sigma^b\boldsymbol{\sigma}_3=\mathbf{0} \quad \text{on } x_3=0, \tag{28c}$$
$$\mathbf{I}_u^t\mathbf{u}+\mathbf{I}_\sigma^t\boldsymbol{\sigma}_3=\mathbf{0} \quad \text{on } x_3=h, |x_1-L/2|>c, \tag{28d}$$
$$\mathbf{I}_u^t\mathbf{u}+\mathbf{I}_\sigma^t\boldsymbol{\sigma}_3'=[\,0\quad 0\quad g(x_1)\,]^{\mathrm{T}} \quad \text{on } x_3=h, |x_1-L/2|\leqslant c, \tag{28e}$$

where $(\boldsymbol{\sigma}_3')_1=(\mu\sin^2\theta+\sin\theta\cos\theta)\sigma_{11}+(\mu\cos^2\theta-\sin\theta\cos\theta)\sigma_{33}-(\mu\sin 2\theta+\cos 2\theta)\sigma_{31}$. Instead of satisfying pointwise boundary conditions (28) and continuity conditions (8), we enforce them in an average (or Fourier's) sense as detailed below:

$$\int_{-l^{(n)}}^{l^{(n)}}\left\{\mathbf{I}_u^{nt}\mathbf{u}^{(n)}(x_1^{(n)},h)+\mathbf{I}_\sigma^{nt}\boldsymbol{\sigma}_3^{(n)}(x_1^{(n)},h)-\mathbf{g}^{nt}(x_1^{(n)})\right\}\exp\left(j\frac{\mathrm{i}\pi x_1^{(n)}}{l^{(n)}}\right)dx_1^{(n)}=\mathbf{0}, \tag{29a}$$

$$\int_{-l^{(n)}}^{l^{(n)}}\left\{\mathbf{I}_u^{nb}\mathbf{u}^{(n)}(x_1^{(n)},0)+\mathbf{I}_\sigma^{nb}\boldsymbol{\sigma}_3^{(n)}(x_1^{(n)},0)-\mathbf{g}^{nb}(x_1^{(n)})\right\}\exp\left(j\frac{\mathrm{i}\pi x_1^{(n)}}{l^{(n)}}\right)\mathrm{d}x_1^{(n)}=\mathbf{0}, \quad j=0,1,2\ldots, \quad n=1,2,3, \tag{29b}$$

$$\int_{-h}^{h}\left\{\mathbf{I}_u^l\mathbf{u}^{(1)}(0,x_3)+\mathbf{I}_\sigma^l\boldsymbol{\sigma}_1^{(1)}(0,x_3)-\mathbf{g}^l(x_3)\right\}\exp\left(j\frac{\mathrm{i}\pi x_3}{h}\right)\mathrm{d}x_3=\mathbf{0}, \tag{29c}$$

$$\int_{-h}^{h}\left\{\mathbf{I}_u^r\mathbf{u}^{(3)}(0,x_3)+\mathbf{I}_\sigma^r\boldsymbol{\sigma}_1^{(3)}(0,x_3)-\mathbf{g}^r(x_3)\right\}\exp\left(j\frac{\mathrm{i}\pi x_3}{h}\right)\mathrm{d}x_3=\mathbf{0}, \quad j=0,1,2\ldots, \tag{29d}$$

$$\int_{-h}^{h}\left\{\mathbf{u}^{(n)}(l^{(n)},x_3)-\mathbf{u}^{(n+1)}(0,x_3)\right\}\exp\left(j\frac{\mathrm{i}\pi x_3}{h}\right)\mathrm{d}x_3=\mathbf{0}, \tag{30a}$$

$$\int_{-h}^{h}\left\{\boldsymbol{\sigma}_1^{(n)}(l^{(n)},x_3)-\boldsymbol{\sigma}_1^{(n+1)}(0,x_3)\right\}\exp\left(j\frac{\mathrm{i}\pi x_3}{h}\right)\mathrm{d}x_3=\mathbf{0}, \quad j=0,1,2\ldots, \quad n=1,2. \tag{30b}$$

Here, $l^{(1)}=l^{(3)}=(L/2)-c$, $l^{(2)}=2c$; $\mathbf{I}_u^{1t}=\mathbf{I}_u^{3t}=\mathrm{diag}[0,1,0]$, $\mathbf{I}_\sigma^{1t}=\mathbf{I}_\sigma^{3t}=\mathrm{diag}[1,0,1]$, $\mathbf{I}_u^{2t}=\mathrm{diag}[0,1,1]$, $\mathbf{I}_\sigma^{2t}=\mathrm{diag}[1,0,0]$; $\mathbf{I}_u^l=\mathbf{I}_u^r=\mathrm{diag}[0,1,0]$, $\mathbf{I}_\sigma^l=\mathbf{I}_\sigma^r=\mathrm{diag}[1,0,1]$; $\mathbf{I}_\sigma^{1b}=\mathbf{I}_\sigma^{2b}=\mathbf{I}_\sigma^{3b}=\mathrm{diag}[0,0,0]$, $\mathbf{I}_u^{1b}=\mathbf{I}_u^{2b}=\mathbf{I}_u^{3b}=\mathrm{diag}[1,1,1]$; $\mathbf{g}^{2t}(x_1^{(n)})=\mathrm{diag}[0,0,g(x_1)]$, $\mathbf{g}^{1t}(x_1^{(n)})=\mathbf{g}^{3t}(x_1^{(n)})=\mathbf{g}^{1b}(x_1^{(n)})=\mathbf{g}^{2b}(x_1^{(n)})=\mathbf{g}^{3b}(x_1^{(n)})=\mathbf{g}^l(x_3)=\mathbf{g}^r(x_3)=\mathrm{diag}[0,0,0]$.

Eq. (29a) can be directly applied to the indentation problem for a flat punch. However, in order to avoid the appearance of the unknown indentation depth u_0 in boundary conditions for cylindrical or parabolic indenters, we differentiate both sides of Eq. $(5d)_2$ with respect to x_1, and use

$$u_3'^{(2)}(x_1,h)=g'(x_1) \tag{31}$$

as the boundary condition in region II where a prime indicates differentiation with respect to x_1. Thus, in segment II, we enforce

$$\int_{-l^{(2)}}^{l^{(2)}}\left\{\mathbf{I}_{u'}^{2t}\mathbf{u}'^{(2)}(x_1^{(2)},h)+\mathbf{I}_\sigma^{2t}\boldsymbol{\sigma}_3^{(2)}(x_1^{(2)},h)-\mathbf{g}'^{2t}(x_1^{(2)})\right\}\exp\left(j\frac{\mathrm{i}\pi x_1^{(2)}}{l^{(2)}}\right)\mathrm{d}x_1^{(2)}=\mathbf{0}, \tag{29a$*$}$$

where $\mathbf{I}_{u'}^{2t}=\mathrm{diag}[0,0,1]$ and $\mathbf{g}'^{2t}(x_1^{(2)})=\mathrm{diag}[0,0,g'(x_1)]$. Once the problem has been solved, the indentation u_0 can be found from Eq. (29a).

By substituting from Eq. (25) into Eqs. (29) and (30), we determine the unknown parameters $\mathbf{d}^{(n)}$, $\mathbf{v}^{(n)}$, $\mathbf{w}^{(n)}$, $\mathbf{q}_k^{(n)}$, $\mathbf{r}_k^{(n)}$, $\mathbf{s}_m^{(n)}$ and $\mathbf{t}_m^{(n)}$ ($n=1,2,3$; $k=0,1,2,\ldots$; $m=0,1,2,\ldots$). The polynomial and the exponential functions corresponding to each unknown parameter, and the prescribed function $g'(x_1)$ are extended as even functions over the interval $(-l^{(n)},0)$. By truncating m to M in Eqs. (29) and (30), and equating the real and the imaginary parts on both sides of those equations, we obtain the number of real equations equal to the number of real unknowns. To maintain approximately the same period of the largest harmonic on all interfaces and boundaries, we truncate k to $K^{(n)}$ for the n^{th} segment with

$$K^{(n)}=\mathrm{Ceil}\left(M\frac{l^{(n)}}{h}\right), \tag{32}$$

where Ceil$(*)$ gives the smallest integer greater than or equal to $*$.

Based on the afore-stated equations, we have developed a computer code in MATLAB to solve the problem. As described in the following section, the code has been verified by comparing computed results for three problems with those available in the literature.

4. Verification of the algorithm

We determine the number of terms to be retained in the series solution (cf. Eq. (23)) and verify our algorithm as follows. We first obtain a converged solution for a layer made of an orthotropic material with principal material axes coincident with the rectangular Cartesian coordinate axes exhibited in Fig. 1, and compare presently computed results with those available in the literature. Subsequently, we verify the code for an isotropic layer. In Section 6, results for a flat rigid punch contacting a linear elastic layer are compared with those available in the literature.

4.1. Indentation of an orthotropic half space by a smooth rigid parabolic indenter

We compare our results with the analytical solution of Hwu and Fan (1998) for the indentation of an orthotropic half-space by the smooth rigid parabolic indenter, $x_3 = [(x_1 - L/2)^2]/2R$ where R is the radius of curvature of the indenter at the point $(L/2,0)$.

For plane strain deformations in the x_1x_3-plane, Hooke's law for an orthotropic material can be written as

$$\begin{Bmatrix} \sigma_{11} \\ \sigma_{33} \\ \sigma_{13} \end{Bmatrix} = \begin{bmatrix} C_{11} & C_{13} & 0 \\ C_{13} & C_{33} & 0 \\ 0 & 0 & C_{55} \end{bmatrix} \begin{Bmatrix} e_{11} \\ e_{33} \\ 2e_{13} \end{Bmatrix}, \tag{33}$$

where

$$\begin{aligned} &C_{11} = \frac{1 - v_{23}v_{32}}{\Delta} E_1, \quad C_{33} = \frac{1 - v_{12}v_{21}}{\Delta} E_3, \\ &C_{13} = \frac{v_{31} + v_{21}v_{32}}{\Delta} E_1 = \frac{v_{13} + v_{12}v_{23}}{\Delta} E_3, \quad C_{55} = G_{31}, \\ &\Delta = 1 - v_{12}v_{21} - v_{23}v_{32} - v_{31}v_{13} - 2v_{21}v_{32}v_{13}. \end{aligned} \tag{34}$$

Here, E_i is Young's modulus in the x_i-direction, G_{31} is the shear modulus in the x_3x_1-plane, and

$$v_{ij} = -\frac{\text{normal strain in the } x_j\text{-direction}}{\text{normal strain in the } x_i\text{-direction}} \tag{35}$$

for a uniaxial stress applied along the x_i-direction. According to Hwu and Fan (1998), the normal stress, σ_{33}, between the indenter and the half space with the material principal axes coincident with the rectangular Cartesian coordinate axes is given by

$$\sigma_{33} = -\frac{1}{\beta R}\sqrt{c^2 - (x_1 - L/2)^2}, \quad |x_1 - L/2| < c, \tag{36}$$

where

$$\frac{1}{\beta} = \alpha_2 \kappa_2 E_3, \tag{37a}$$

$$\alpha_2 = (1 - v_{23}v_{32})^{-1/2}, \tag{37b}$$

$$\kappa_2 = \left(E_3/G_{31} + 2\eta_1\sqrt{E_3/E_1}\right)^{-1/2}, \tag{37c}$$

$$\eta_1 = \sqrt{(1 - v_{12}v_{21})(1 - v_{23}v_{32})} - \sqrt{(v_{31} + v_{21}v_{32})(v_{13} + v_{23}v_{12})}. \tag{37d}$$

In order to compute numerical results we assign following values to various material and geometric parameters:

$$\begin{aligned} &E_1 = 25.0\ \text{GPa}, \quad E_2 = E_3 = 1.0\ \text{GPa}, \quad G_{23} = 0.2\ \text{GPa}, \\ &G_{12} = G_{31} = 0.5\ \text{GPa}, \quad v_{12} = v_{23} = v_{13} = 0.25, \\ &L = 1.0\ \text{m}, \quad h = 0.4\ \text{m}, \quad R = 0.5\ \text{m}, \quad 2c = 0.1\ \text{m}. \end{aligned} \tag{38}$$

Then $v_{21} = v_{31} = 0.01$ and $v_{32} = 0.25$ can be calculated from values of parameters listed in Eq. (38) and the relations $E_i/v_{ij} = E_j/v_{ji}$ (no sum on i and j). Since $2c/L = 0.1$, it is reasonable to assume that null tractions applied on the left and the right vertical surfaces do not influence the solution in the vicinity of the contact region. The computed value of u_0 was found to be less than $0.1h$ signifying thereby the applicability of the analytical solution for the half space to the present problem. We have compared in Fig. 2 the pressure distribution on the contact surface for the analytical solution of Hwu and Fan (1998) with the presently computed one by setting $K = 500$ in the series solution represented by Eqs. (23)–(25). It is clear that the two pressure distributions agree well with each other, and the maximum error in the computed pressure for $(x_1 - L/2) < 0.9c$ is 2.7%.

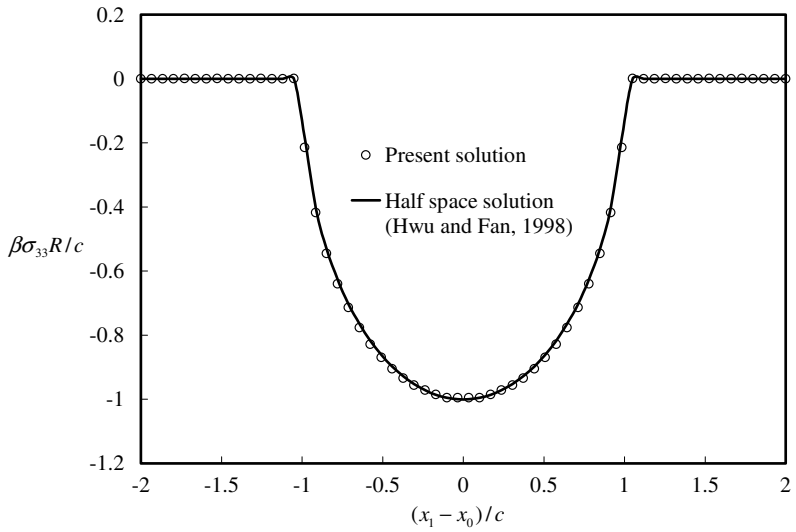

Fig. 2. For an orthotropic layer, comparison of the presently computed pressure distribution on the contact surface with that of Hwu and Fan (1998).

4.2. Indentation of an isotropic elastic layer by a smooth rigid cylinder

For $c/h < 1$, Meijers (1968) has derived the following expression for the pressure on the contact surface between a smooth rigid circular cylinder of radius R and an isotropic elastic layer perfectly bonded to a rigid base:

$$\sigma_{33} = -\frac{E}{2(1-\nu^2)}\frac{\sqrt{c^2-(x_1-L/2)^2}}{R}\left[1+\frac{1}{8}\alpha_1\left(\frac{c}{h}\right)^2+\frac{1}{64}(\alpha_1^2+5\alpha_2+4\alpha_2(x_1-L/2)^2/c^2)\left(\frac{c}{h}\right)^4\right], \quad |x_1-L/2|<c, \tag{39}$$

where E equals Young's modulus, and for Poisson's ratio $\nu = 0.3$, $\alpha_1 = 5.7278$ and $\alpha_2 = -7.8479$. Values of parameters α_1 and α_2 depend upon the value of Poisson's ratio, and have been computed by Meijers (1968) for $\nu = 0.0, 0.3, 0.4, 0.45, 0.48$ and 0.5. For values of c/h between 0 and 0.7, Meijers (1968) has shown that Eq. (39) gives converged values of the pressure distribution on the contact surface.

We solve the problem by the Stroh formalism given above and compare our solution with that of Meijers (1968). For an isotropic linear elastic material, eigenvalues and eigenvectors of the eigenvalue problem defined by Eq. (14) are

$$p_1 = p_2 = p_3 = \mathrm{i}, \quad p_4 = p_5 = p_6 = -\mathrm{i}, \tag{40a}$$

$$\begin{bmatrix} 1 & \mathrm{i} & 0 \\ \mathrm{i} & -1 & 0 \\ 0 & 0 & 0 \end{bmatrix}\mathbf{a} = \mathbf{0}, \tag{40b}$$

$$\mathbf{b}_\alpha = (\mathbf{R}^{\mathrm{T}} + p\mathbf{T})\mathbf{a}_\alpha. \tag{40c}$$

That is, there are only two independent eigenvectors for isotropic materials, and the parameter β in Eq. (37) is given by $\beta = [2(1-\nu^2)]/E$. Ting (1982) has discussed modifications needed to get general solutions for an isotropic material. However, in stead of following this rather lengthy procedure, we alter values of elastic constants by ±1% to get unequal eigenvalues of the eigenvalue problem defined by Eq. (14).

As shown in Fig. 3, the presently computed pressure distribution on the contact surface matches well with that given by Meijers (1968), and the maximum deviation between the two pressure distributions for $(x_1 - L/2) < 0.9c$ is 6.0%.

4.3. Effect of number of terms in the series solution

The effect of the number of terms in the series solution given by Eq. (23) is investigated by comparing, for the above two problems, the total axial load (cf. Eq. (7a)) from the analytical solution with that obtained from the numerical solution. For an orthotropic half space indented by a smooth parabolic indenter, Eqs. (7a) and (36) give

$$P_{\mathrm{ortho}} = \frac{\pi c^2}{2\beta R}. \tag{41}$$

For an isotropic linear elastic layer bonded to a rigid substrate, we conclude from Eqs. (7a) and (39) that

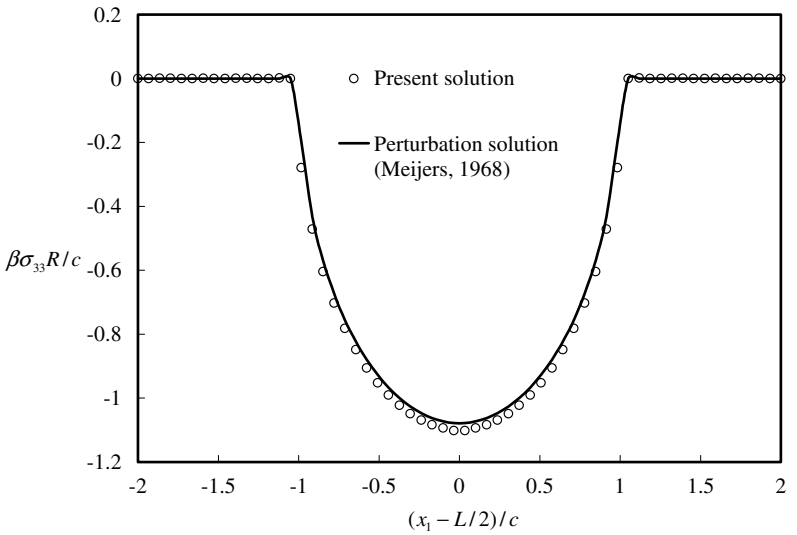

Fig. 3. For an isotropic layer with $\nu = 0.3$, $c/h = 1/3$, $c/L = 0.05$, comparison of the presently computed pressure distribution on the contact surface with that of Meijers (1968).

$$P_{\text{iso}} = \frac{\pi E c^2}{4(1-\nu^2)R}\left[1 + \frac{1}{8}\alpha_1\left(\frac{c}{h}\right)^2 + \frac{1}{64}(\alpha_1^2 + 6\alpha_2)\left(\frac{c}{h}\right)^4\right]. \tag{42}$$

Upon substitution of $\beta = 2(1-\nu^2)/E$ in Eq. (41), we see that Eqs. (41) and (42) give the same indentation load for an isotropic half space only when $c/h \ll 1$ so that the term in brackets on the right-hand side of Eq. (42) equals 1.

For different values of $K = \sum_{n=1}^{3} K^{(n)}$, we have listed in Table 2.1 the percentage error between the axial loads computed from Eqs. (22) and (23) and their values obtained from the solution of the corresponding problems with the present method. It is clear that the retention of 400 terms in the series solution for an orthotropic layer gives an error in the axial load of about 1.9%. However, for an isotropic layer, one needs to retain more terms because of the occurrence of nearly equal eigenvalues. Of course, errors listed in Table 1 in the total axial load do not provide any information about the error in the local stresses, strains and displacements. In keeping with the goal of finding a relation between the axial load and the indentation, we accept 1.9% error in the axial load, and compute results presented herein with $K = 400$.

5. Parametric studies

For an orthotropic layer bonded to a rigid substrate and indented by a smooth parabolic rigid indenter, we first delineate the effect of varying geometric parameters and then material parameters. When studying the effect of geometric parameters, we assign values to material parameters listed in Eq. (38); thus $\beta = 1.49\ \text{GPa}^{-1}$. We also have studied the influence of the coefficient of friction between the two contacting surfaces on the axial load and the depth of indentation.

5.1. Geometric parameters

There are four geometric parameters, namely, the radius R of the indenter, the half contact width c, the length L and the thickness h of the deformable layer. Recall that the indentation u_0 is computed after the contact problem has been solved. Eqs. (36) and (39) suggest that lengths should be non-dimensionalized with the semi-contact width c. We thus need to study the effect of varying L/c, h/c and R/c.

Table 1
Effect of number of terms in the series solution on the percentage error in the axial loads for the contact problems involving layers made of orthotropic and isotropic materials

Orthotropic layer ($c/h = 0.125$, $c/L = 0.05$; parabolic indenter)		Isotropic layer ($c/h = 1/3$, $c/L = 0.05$, $\nu = 0.3$; circular cylindrical indenter)	
Number, K, of terms in the series solution	%Error $= 100 \times \lvert P - P_{\text{ortho}}\rvert / P_{\text{ortho}}$	Number, K, of terms in the series solution	%Error $= 100 \times \lvert P - P_{\text{iso}}\rvert / P_{\text{iso}}$
400	1.9	400	7.0
600	1.3	800	5.0
800	1.0	1200	4.1
1000	0.8	1600	3.5

5.1.1. Effect of changing c/h

With c, L and R kept fixed so that $c/L = 0.05$ and $c/R = 0.05$, and varying the layer thickness h, we have plotted in Fig. 4 the variation with c/h of the non-dimensional axial load, P, and the non-dimensional indentation u_0/h. It is clear that for $c/h > 0.6$, P for the finite thickness layer deviates from that for the half-space by at least 5%. Both the non-dimensional indentation and the non-dimensional axial load increase monotonically with an increase in c/h. Whereas the slope of the P vs. c/h curve continues to increase with an increase in the value of c/h, that of u_0/h vs. c/h monotonically decreases at least in the range of values of c/h studied herein. For $u_0/h < 0.1$, the difference between the current value of P and that derived from the half-space solution can be neglected. Thus the indented sample can be regarded as a half space if the indentation depth is less than 10% of the sample thickness.

The least squares fit to the computed values of $\beta P/2c$ vs. c/h is

$$\frac{\beta P}{2c} = 0.0393 - 0.0003\left(\frac{c}{h}\right) - 0.007\left(\frac{c}{h}\right)^2 + 0.0344\left(\frac{c}{h}\right)^3 - 0.0182\left(\frac{c}{h}\right)^4. \tag{43}$$

It is evident from the plot of Eq. (43) included in Fig. 4 that it provides a very good fit to the computed values. For $c/h \leqslant 0.1$, one can take $\beta P/2c = 0.0393$.

5.1.2. Effect of changing c/R

We now set $c/L = 0.05$ and $c/h = 0.5$, and vary c/R; the corresponding axial load, P, is plotted in Fig. 5. Since c/R can reach 0.5 in this case, we calculate the axial load P by both Eqs. (7a) and (7b). Recall that for the half space P is a linear function of c/R with slope equal to $\pi/4$; cf. Eq. (41). For the finite thickness of the orthotropic layer, the slope of the P vs. c/R curve with P computed by using Eq. (7b) is higher than $\pi/4$; the axial load P given by Eq. (7a) is not a linear function of c/R for large values of c/R.

5.1.3. Effect of changing c/L

It is clear from results depicted in Fig. 6 that for $0.05 < c/L < 0.2$, the ratio c/L has virtually no effect on both the non-dimensional axial load $\beta P/2c$ and the non-dimensional indentation u_0/h. Whereas the non-dimensional axial load equals 0.039 for the half space, it equals 0.042 for the finite thickness layer. However, for $c/L > 0.25$, the non-dimensional axial load for the finite thickness layer is much larger than that for the half space.

For $0.05 < c/L < 0.2$, u_0/h may be taken to be constant and equal 0.023.

Results plotted in Figs. 4–6 suggest that the half space solution can be used when $u_0/h \leqslant 0.1$, $c/h \leqslant 0.6$, $c/L \leqslant 0.2$ and $c/R \leqslant 0.15$.

5.2. Material parameters

Eq. (36) evinces that the axial load on a parabolic indenter contacting an orthotropic half space depends on the material elasticities through the parameter β. With parameters assigned values listed in Eq. (38), we vary the value of one parameter at a time and determine the corresponding change in the value of β. Results of this exercise, listed in Table 2, illustrate that values of Young's modulus E_3 and of the shear modulus G_{13} significantly affect the value of β. Accordingly, for $c/R = 0.05$, $c/$

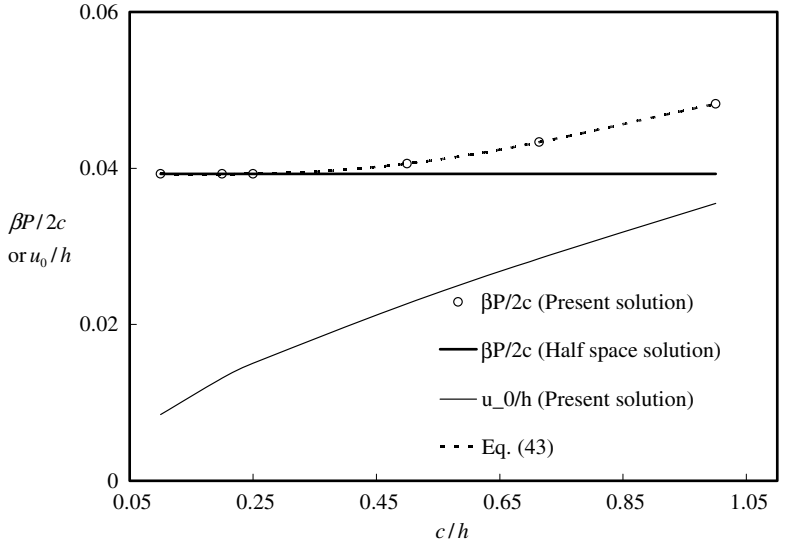

Fig. 4. For $c/L = 0.05$ and $c/R = 0.05$, variation with c/h of the axial load and the depth of indentation.

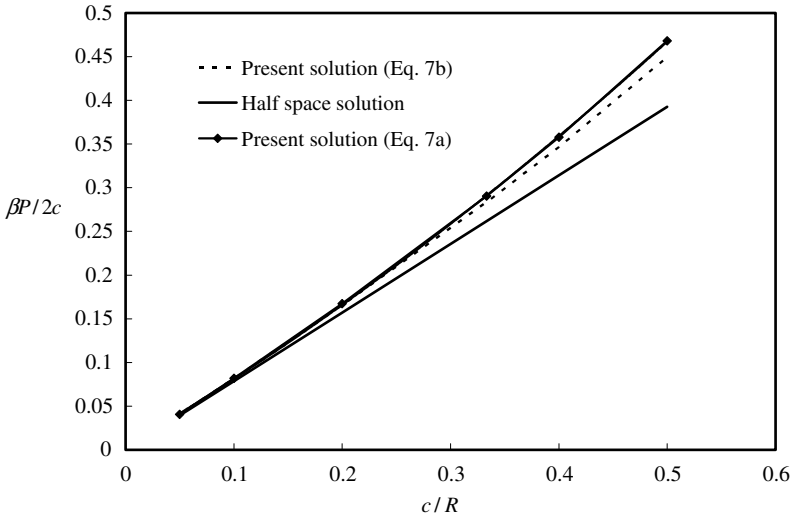

Fig. 5. For $c/L = 0.05$ and $c/h = 0.5$, variation with c/R of the axial load.

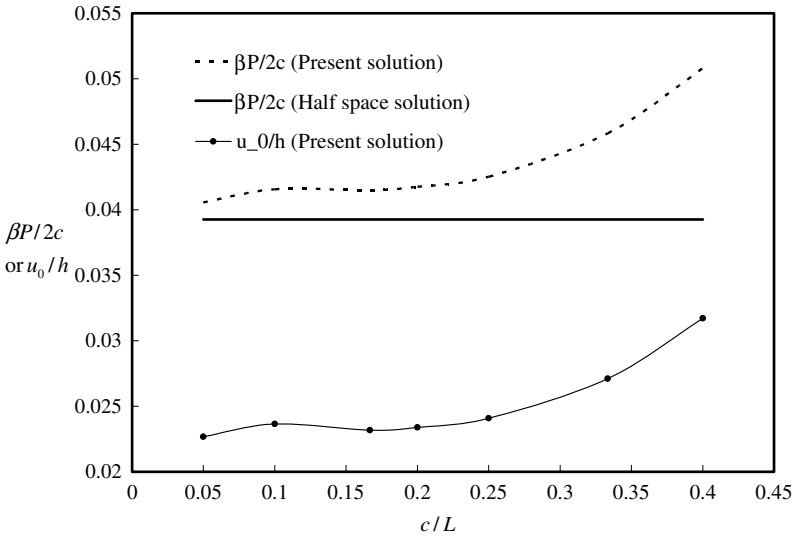

Fig. 6. For $c/h = 0.5$ and $c/R = 0.05$, variation with c/L of the axial load and the depth of indentation.

Table 2
Variation in the value of β with a change in the value of one material parameter

	$\lvert(\beta' - \beta)/\beta'\rvert$		$\lvert(\beta' - \beta)/\beta'\rvert$		$\lvert(\beta' - \beta)/\beta'\rvert$
$E_1' = 10E_1$	0.056	$G_{12}' = 10G_{12}$	0.000	$\nu_{12}' = 0.1\nu_{12}$	0.004
$E_2' = 10E_2$	0.030	$G_{13}' = 10G_{13}$	1.050	$\nu_{13}' = 0.1\nu_{13}$	0.004
$E_3' = 10E_3$	4.364	$G_{23}' = 10G_{23}$	0.000	$\nu_{23}' = 0.1\nu_{23}$	0.031

$L = 0.05$ and $c/h = 0.5$, we have plotted in Figs. 7 and 8 variations with E_3 and G_{13} of the axial load P and of the non-dimensional indentation u_0; values of other material parameters are the same as those given in Eq. (38). The axial load increases nearly linearly as E_3'/E_3 is increased from 1 to 5. Subsequently, for the same value of the half contact width, the axial load increases more rapidly with an increase in E_3'/E_3. For a ten fold increase in E_3'/E_3, the axial load increases by a factor of almost 11. However, the change in the indentation depth is less dramatic as it decreases to nearly one-half of its initial value as E_3 is enhanced by a factor of 10. The increase in G_{13} does not affect the axial load as much as the increase in E_3 does. For example, for $G_{13}'/G_{13} = 10$, the axial load for the same semi-contact width increases by a factor of 1.9 and the depth of indentation by a factor of 1.4.

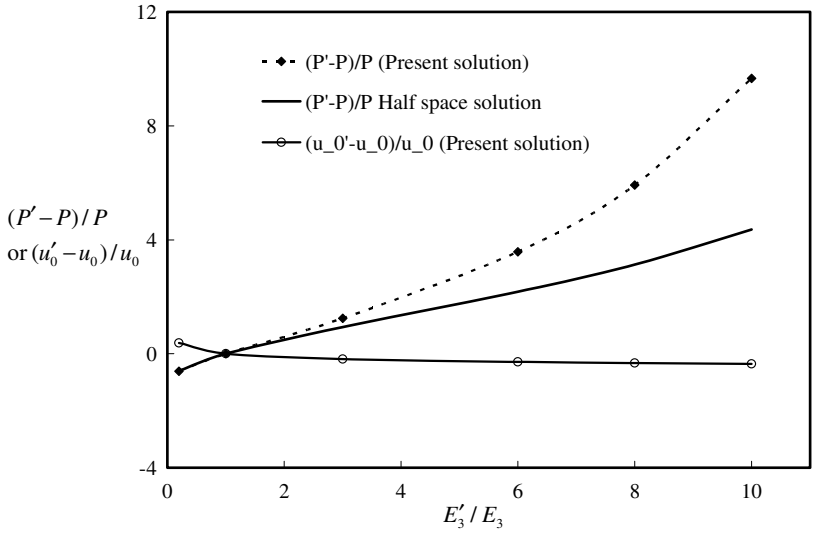

Fig. 7. For $c/R = 0.05$, $c/L = 0.05$ and $c/h = 0.5$, variation with E_3'/E_3 of the axial load and the depth of indentation.

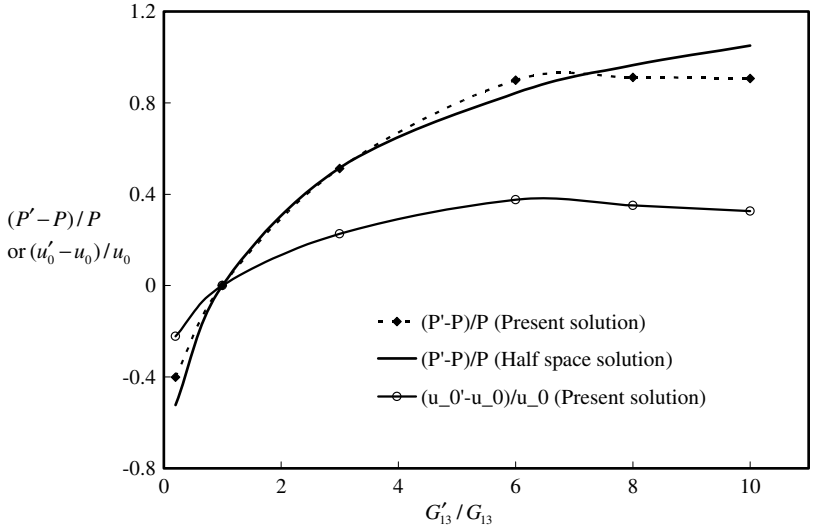

Fig. 8. For $c/R = 0.05$, $c/L = 0.05$ and $c/h = 0.5$, variation with G_{13}'/G_{13} of the axial load and the depth of indentation.

5.3. Coefficient of friction

Results plotted in Fig. 9 suggest that the axial load decreases and the indentation depth increases gradually with an increase in the value of the coefficient of friction μ. When μ is enhanced from 0 to 0.9, the average axial stress $\beta P/2c$ decreases by only 2.6% and the depth of indentation, u_0/h, increases by just 1.1%. Thus it is reasonable to assume smooth contact between the indenter and the layer.

6. Indentation with flat punch

We consider the indentation of an orthotropic layer of finite width L and finite thickness h by a smooth rigid flat indenter with horizontal base of width $2a$ positioned between $x_1 = L/2 - a$, and $x_1 = L/2 + a$, and denote the indentation depth by δ. We have plotted in Figs. 10 and 11 the x_3-displacement and the normal stress σ_{33} acting at points on the top surface of the layer. These results reveal that

$$\sigma_{33}(x_1,h) \sim 1/\sqrt{(L/2+a-x_1)/a}, \quad x_1 \to (L/2+a)^-, \tag{44}$$

$$u_3(x_1,h) \sim \sqrt{(-L/2-a+x_1)/a}, \quad x_1 \to (L/2+a)^+, \tag{45}$$

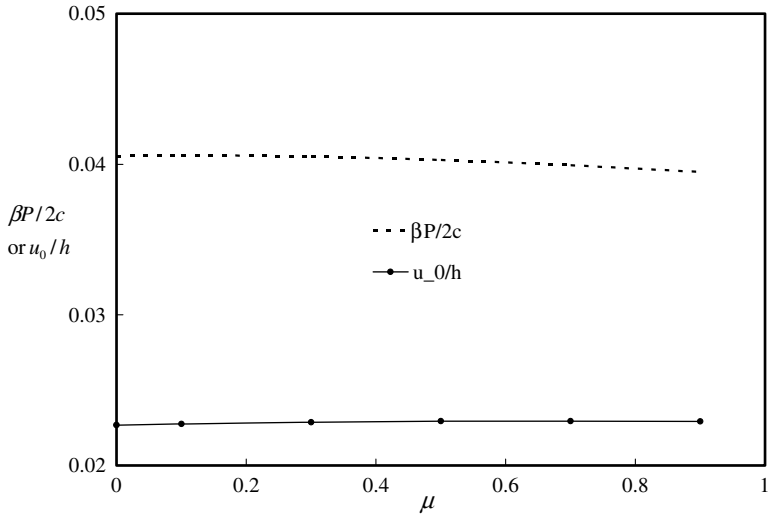

Fig. 9. For $c/R = 0.05$, $c/L = 0.05$ and $c/h = 0.5$, variation with the coefficient of friction of the axial load and the depth of indentation.

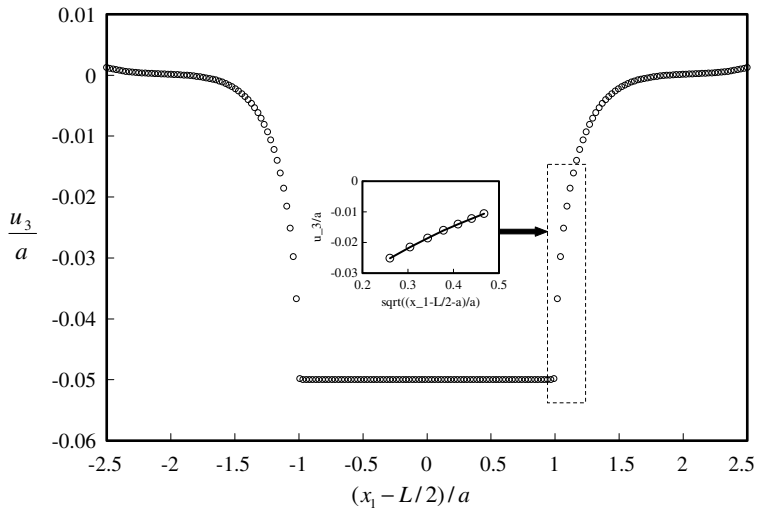

Fig. 10. For $a = 0.2$ m, $L = 1$ m, $h = 0.1$ m and $\delta = 0.01$ m, plot of u_3 on the top surface and singular behavior of u_3 near the edge of the indenter.

which agree with the analytical solution of the indentation of a linear elastic anisotropic half space by a flat indenter (Hwu and Fan, 1998) and the asymptotic solution of the indentation of a linear elastic isotropic layer by a flat indenter (Haider and Holmes, 1995). Except for points near the indenter periphery, the pressure distribution on the indented surface is uniform.

7. Load vs. indentation depth

In indentation experiments, the load versus the indentation depth curve is used to determine an elastic modulus of material of the indented sample. We have plotted these curves for a flat and a cylindrical indenter in Fig. 12 with values of material parameters listed in Eq. (38), the layer width $L = 1.0$ m, the layer thickness $h = 0.1$ m, width $2a$ of the flat indenter = 0.4 m, and the radius R of the cylindrical indenter = 1 m. Whereas for a flat indenter, the load is a linear function of the indentation depth, for a cylindrical indenter the load P is proportional to $u_0^{3/2}$. These results agree qualtitatively with Sneddon's (1965) solution for the indentation of a linear elastic isotropic half space. Thus the indentation modulus defined as the slope of the load vs. the indentation depth curve is a constant for the flat punch, and varies as $u_0^{1/2}$ for the cylindrical indenter.

8. Indentation of a face-centered cubic (FCC) single crystal

Having validated the methodology by favorably comparing computed results with those available in the literature, we now study indentation of a layer of a FCC single crystal of gold (Au) by a rigid cylindrical indenter. We consider three

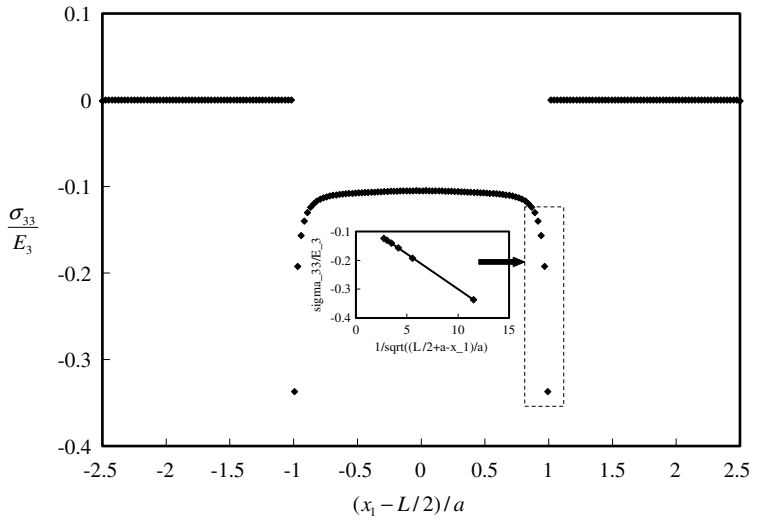

Fig. 11. For $a = 0.2$ m, $L = 1$ m, $h = 0.1$ m and $\delta = 0.01$ m, plot of σ_{33} on the top surface and the singular behavior of σ_{33} near the edge of the indenter.

different orientations of the Au crystal with respect to the global coordinated axes. For coordinate axes coincident with the lattice directions [100], [010] and [001], the matrix of elasticities is given by

$$\mathbf{C}_{001} = \begin{bmatrix} 183 & 159 & 159 & 0 & 0 & 0 \\ 159 & 183 & 159 & 0 & 0 & 0 \\ 159 & 159 & 183 & 0 & 0 & 0 \\ 0 & 0 & 0 & 45 & 0 & 0 \\ 0 & 0 & 0 & 0 & 45 & 0 \\ 0 & 0 & 0 & 0 & 0 & 45 \end{bmatrix} \text{GPa} \tag{46}$$

Thus there are only three independent elastic constants and the form of the matrix looks like that of an orthotropic material with material principal directions coincident with the global coordinate axes. In this case we assume that the indentation is along the [001] direction, and we have denoted the matrix of elastic constants by $\mathbf{C}_{001}$. For single crystals, the indentation in (111) plane is also often studied to observe dislocations (Lilleodden et al., 2003). For this case, the global x_1, x_2, x_3 axes are consistent with the lattice-directions $[1\bar{2}1]$, $[10\bar{1}]$ and [111], as shown in Fig. 13, where the superimposed bar stands for the negative of the quantity. Using the tensor transformation rules, (e.g. see Batra (2005)), the matrix of elastic constants is given by

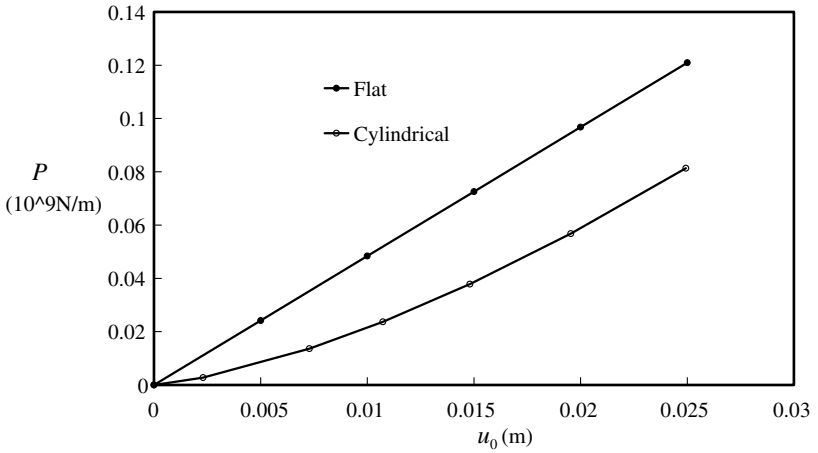

Fig. 12. Load vs. indentation depth curves for flat and cylindrical indenters.

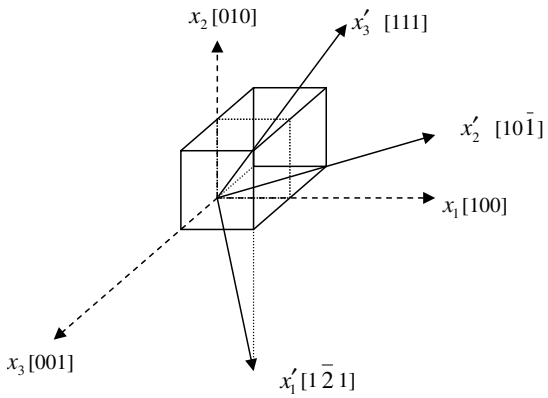

Fig. 13. Axis rotation for (1 1 1) plane indentation of gold lattice.

$$\mathbf{C}_{111} = \begin{bmatrix} 216 & 148 & 137 & 0 & 15.6 & 0 \\ 148 & 216 & 137 & 0 & -15.6 & 0 \\ 137 & 137 & 227 & 0 & 0 & 0 \\ 0 & 0 & 0 & 23 & 0 & -15.6 \\ 15.6 & -15.6 & 0 & 0 & 23 & 0 \\ 0 & 0 & 0 & -15.6 & 0 & 34 \end{bmatrix} \text{GPa} \tag{47}$$

whose form is quite different from that for an orthotropic material with material principal directions coincident with the global coordinate axes. We also consider a crystal orientation for which the global x_1,x_2,x_3 coordinate axes are along the lattice-directions [1 3 1], [1$\bar{1}$2] and [7$\bar{1}\bar{4}$], respectively, and the matrix of elastic constants with respect to the global axes is

$$\mathbf{C}_{7\bar{1}\bar{4}} = \begin{bmatrix} 203.7 & 145.0 & 152.3 & -2.4 & 5.3 & 17.7 \\ 145.0 & 216.0 & 140.0 & 13.3 & 4.9 & -8.1 \\ 152.3 & 140.0 & 208.7 & -10.9 & -10.2 & -9.6 \\ -2.4 & 13.3 & -10.9 & 26.0 & -9.6 & 4.9 \\ 5.3 & 4.9 & -10.2 & -9.6 & 38.3 & -2.4 \\ 17.7 & -8.1 & -9.6 & 4.9 & -2.4 & 31.0 \end{bmatrix} \text{GPa}. \tag{48}$$

The matrix $\mathbf{C}_{7\bar{1}\bar{4}}$ has all elements non-zero and thus corresponds to that of a general anisotropic material.

In Fig. 14 we have plotted the load-displacement curves for the three cases, i.e., the indentation of the Au crystal in (0 0 1), (1 1 1) and (7$\bar{1}\bar{4}$) plane by a rigid cylinder of radius 40 Å. The dimensions of the layer are set as L = 204 Å, h = 20 Å. Each problem is solved by assuming that the Au crystal can be regarded as a continuum and the linear elasticity theory applies. For indentation along the (111) plane, we also use Yang and Sun's assumption (1982) to compute the load-indentation curve.

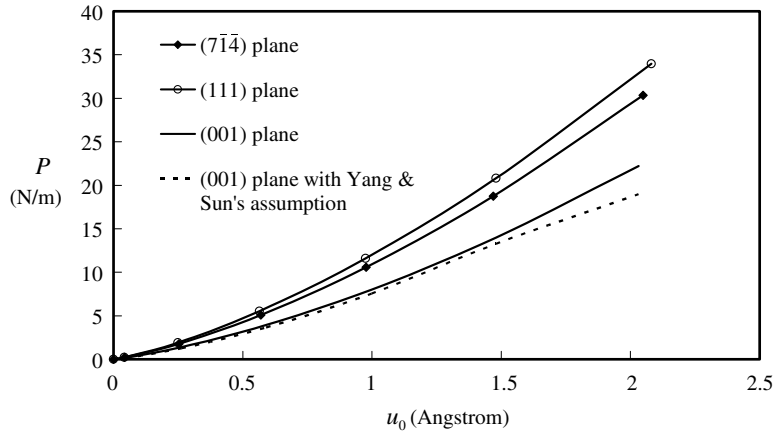

Fig. 14. Load vs. indentation depth curves for indentation of gold crystal.

Yang and Sun (1982) proposed that the indentation load for a layer made of an orthotropic material can be deduced from the expression for an isotropic material by replacing $E/(1-\nu^2)$ for the isotropic material by Young's modulus E_3 in the indentation direction of the anisotropic material. For the plane strain problem being studied herein, this is equivalent to replacing $1/\beta = E/[2(1-\nu^2)]$ in Eq. (42) by E_3 of the orthotropic material. Values of α_1 and α_2 in Eq. (42) are obtained by interpolating values given in Table 1 of Meijers' paper with $\nu = 0.465$ for gold. The P vs. u_0 curve identified in Fig. 14 as the one obtained with Yang and Sun's assumption is the plot of values derived from Eq. (42).

From the load vs. indentation curves exhibited in Fig. 14, we conclude that the anisotropy of the material has a noticeable effect on the load required to cause the same indentation. For indentation equal to 10% of the layer thickness, the error caused by Yang and Sun's (1982) is 14% and it increases with an increase in the indentation. We note that for indentation of an orthotropic material by a spherical indenter, Swanson (2005) showed that the indentation load obtained with the Yang and Sun approximation can have errors of 22%.

9. Discussion

As illustrated in Vel and Batra (2000, 2001) the present technique can also be used when the indented body is comprised of several layers made of different anisotropic materials. The body is divided into different regions with continuity of displacements and tractions (e.g. cf. Eqs. (8a)–(8d) satisfied at interfaces between adjoining regions. The technique can also be used to study problems when there is imperfect bond between adjoining layers provided that the friction law between adjoining layers is known. Problems involving cracks between adjoining layers can also be studied by simulating crack surfaces traction free. These problems become more challenging if a crack closes. Furthermore, various boundary conditions at the edges can be well simulated; e.g. see Vel and Batra (1999)

Results presented herein can be used as benchmarks to validate solutions obtained by other techniques such as the finite element method.

The focus here has been to describe and establish the technique, and show that results computed with it agree well with those available in the literature derived by using different methods. We have also provided results for the indentation of a FCC crystal with the plane of indentation not coincident with the planes of material symmetry. The elasticity matrix for these problems is similar to that of a general anisotropic material.

10. Conclusions

We have used the Stroh formalism to study infinitesimal deformations of a linear elastic anisotropic layer perfectly bonded to a rigid substrate and statically deformed by either a cylindrical or a flat indenter. The problem is formulated in terms of the a priori unknown semi-contact width c. Boundary conditions on all surfaces are satisfied in the sense of the Fourier solution. Computed axial loads for the indentation of an orthotropic layer by a smooth parabolic cylinder and of an isotropic layer by a smooth circular cylinder are found to compare well with the corresponding solutions for half spaces available in the literature. The influence on the axial load of various geometric and material parameters has been delineated. These results have revealed that the non-dimensional axial load is independent of c/L for $c/L < 0.2$ where $2c$ equals the contact width and L the width of the layer. For an indenter of radius R, the non-dimensional axial load varies linearly with c/R as for a half space. However, the slope of the axial load vs. the indentation line for the finite thickness layer is higher than that of the line for the half space. The coefficient of friction between the layer material and the indenter has very little effect on the axial load required to indent the layer. Among the material elasticities of the orthotropic layer, the elastic modulus in the direction of indentation has the most effect on the axial load and that is followed by the shear modulus in the plane of deformation. Values of Poisson's ratios have negligible effects on the axial load.

The half space solution can be used for indentation depths less than one-tenth the layer thickness h provided that $c/h \leqslant 0.4$, $c/L \leqslant 0.2$ and $c/R \leqslant 0.15$ where L is the length of the layer and R the indenter radius.

Results for a flat punch indenting a layer comprised of a linear elastic anisotropic material are found to match well with results available in the literature.

The problem formulation is valid for a general anisotropic material, indenters of different profiles, different boundary conditions at the edges of the indented layer, and the indented body comprised of several perfectly or imperfectly bonded layers.

Acknowledgements

This work was partially supported by the ONR Grant N00014-06-1-0567 to Virginia Polytechnic Institute and State University with Dr. Y.D.S. Rajapakse as the program manager. Views expressed in the paper are those of authors and neither of the funding agency nor of VPI&SU.

References

Aboussaleh, M., Boukhili, R., 1998. The contact behavior between laminated composites and rigid impactors. Composite Structures 43, 165–178.
Batra, R.C., 2005. Elements of Continuum Mechanics. AIAA, Reston.
Barnett, D.M., Lothe, J., 1975. Line force loadings on anisotropic half-spaces and wedges. Physica Norvegica 8, 13–22.

Eshelby, J.D., Read, W.T., Schockley, W., 1953. Anisotropic elasticity with applications to dislocation theory. Acta Metallurgica 1, 251–259.
Fan, C.W., Hwu, C., 1996. Punch problems for anisotropic elastic half-plane. Journal of Applied Mechanics 63, 69–76.
Green, A.E., Zerna, W., 1954. Theoretical Elasticity. Oxford University Press, Oxford.
Haider, M.A., Holmes, M.H., 1995. Indentation of a thin compressible elastic layer: approximate analytic and numerical solutions for rigid flat indenters. Journal of the Mechanics and Physics of Solids 43, 1199–1219.
Hwu, C., Fan, C.W., 1998. Sliding punches with or without friction along the surface of an anisotropic elastic half-plane. Quarterly Journal of Mechanics and Applied Mathematics 51, 159–177.
Johnson, K.L., 1985. Contact Mechanics. Cambridge University Press, Cambridge, UK.
Kuo, C.H., Keer, L.M., 1992. Contact stress analysis of a layered transversely isotropic half-space. ASME Journal of Tribology 114, 253–262.
Lilleodden, E.T., Zimmerman, S.M., Foiles, S.M., Nix, W.D., 2003. Atomistic simulations of elastic deformation and dislocation nucleation during nanoindentation. Journal of the Mechanics and Physics of Solids 51, 901–920.
Lin, Y., Ovaert, T.C., 2004. A rough surface contact model for general anisotropic materials. Journal of Tribology 126, 41–49.
Lovell, M., Morrow, C., 2006. Three-dimensional contact analysis of anisotropic coated surfaces. Tribology Transactions 49 (1), 33–38.
Meijers, P., 1968. The contact problem of a rigid cylinder on an elastic layer. Applied Science Resources 18, 353–383.
Muskhelishvili, N.I., 1954. Some basic problems of the mathematical theory of elasticity. Noordhoff. Groningen, The Netherlands.
Ning, X., Lovell, M.R., Slaughter, W.S., 2003. Two-dimensional anisotropic contact behavior of unidirectional continuous FRP Composites. Journal of Tribology 125 (2), 457–461.
Sneddon, I.N., 1965. The relation between load and penetration in the axisymmetric Boussinesq problem for a punch of arbitrary profile. International Journal of Engineering Science 3, 47–57.
Srinivas, S., Rao, A.K., 1970. Bending, vibration and buckling of simply supported thick orthotropic rectangular plates and laminates. International Journal of Solids and Structures 6, 1463–1481.
Stroh, A.N., 1958. Dislocations and cracks in anisotropic elasticity. Philosophical Magazine 7, 625–646.
Stroh, A.N., 1962. Steady state problems in anisotropic elasticity. Journal of Mathematics and Physics 41, 77–103.
Swadener, J.G., Pharr, G.M., 2001. Indentation of elastically anisotropic half-spaces by cones and parabolae of revolution. Philosophical Magazine A 81 (2), 447–466.
Swanson, S.R., 2004. Hertzian contact of orthotropic materials. International Journal of Solids and Structures 41, 1945–1959.
Swanson, S.R., 2005. Contact deformation and stress in orthotropic plates. Composites Part A: Manufacturing and Applied Science 36, 1421–1429.
Tan, T.M., Sun, C.T., 1985. Use of statical indentation laws in the impact analysis of laminated composite plates. Journal of Applied Mechanics 5, 6–12.
Ting, T.C.T., 1996. Anisotropic Elasticity: Theory and Applications. Oxford University Press, Oxford.
Ting, T.C.T., 1982. Effects of change of reference coordinates on the stress analyses of anisotropic elastic materials. International Journal of Solids and Structures 18, 139–152.
Töyräs, T.L., Niinimäki, M., Lindgren, R., Nieminen, M.T., Kiviranta, I., Jurvelin, J.S., 2001. Estimation of the Young's modulus of articular cartilage using an arthroscopic indentation instrument and ultrasonic measurement of tissue thickness. Journal of Biomechanics 34, 251–256.
Turner, J.R., 1966. Contact on a transversely isotropic half-space, or between two transversely isotropic bodies. International Journal of Solids and Structures 16, 409–419.
Vel, S.S., Batra, R.C., 1999. Analytical solutions for rectangular thick laminated plates subjected to arbitrary boundary conditions. AIAA Journal 37, 1464–1473.
Vel, S.S., Batra, R.C., 2000. The generalized plane strain deformations of thick anisotropic composite laminated plates. International Journal of Solids and Structures 37, 715–733.
Vel, S.S., Batra, R.C., 2001. Closure to the generalized plane strain deformations of thick anisotropic composite laminated plates. International Journal of Solids and Structures 38, 483–489.
Willis, J.R., 1966. Hertzian contact of anisotropic bodies. Journal of the Mechanics and Physics of Solids 14, 163–176.
Wu, E., Yen, C., 1994. The contact behavior between laminated composite plates and rigid spheres. Journal of Applied Mechanics 61, 60–66.
Yang, S.H., Sun, C.T., 1982. Indentation law for composite laminates. In: Daniel, I.M. (Ed.), Composite Materials: Testing and Design, Proc. of the 6th Conference, ASTM STP 787, pp. 425–449.